Journal of Constructional Steel Research 147 (2018) 477–487

Contents lists available at ScienceDirect

Journal of Constructional Steel Research

Experimental study on the hysteretic behavior of steel plate shear wall with unequal length slits

Jinyu Lu [a,b,*], Shunji Yu [b], Jun Xia [c], Xudong Qiao [b], Yi Tang [b]

[a] Key Lab of Concrete and Prestressed Concrete Structures of Ministry of Education, Southeast University, Nanjing 210096, China
[b] School of Civil Engineering, Southeast University, Nanjing 210096, China
[c] Department of Civil Engineering, Xi'an Jiaotong-Liverpool University, Suzhou, 215123, China

ARTICLE INFO

Article history:
Received 7 January 2018
Received in revised form 12 April 2018
Accepted 2 May 2018
Available online 15 May 2018

Keywords:
Steel plate shear wall
Unequal length slits
Hysteretic behavior
Low cycle tests
Finite element analysis

ABSTRACT

A steel plate shear wall with slits (SPSWS) is an effective anti-seismic component element, which owns good ductility and energy dissipation capacity. The infill steel plate is divided into flexural links by slits, which changes the path of conducting force. As a result, the SPSWSs obtain higher energy dissipation capacity and better ductility compared with conventional steel plate shear walls. However, both tests and finite element method (FEM) analysis have shown that the slits lower the ultimate bearing capacity and the lateral stiffness of the steel plate shear wall. In this case, two steel plate shear walls with unequal length slits (SPSWUS), i.e. papilionaceous SPSWUS and fusiform SPSWUS, are proposed and analyzed in this paper. Four 1/3-scaled test specimens are designed for the experimental study. Two of the specimens are SPSWUSs, and the other two are traditional SPSWSs. Testing of the systems were performed under cyclic lateral loading. Results show that SPSWUS has rather high energy dissipation capacity and good ductility as well as relatively high lateral stiffness and ultimate bearing capacity when compared with the traditional SPSWS. Experimental results correlate well with those from the finite element analysis, which validates the finite element model.

1. Introduction

Steel plate shear walls, as a new type of lateral resistant system, have been proven to exhibit high lateral stiffness and excellent ultimate bearing capacity in high rise buildings [1]. Ge et al. [2] conducted a shaking table test of a 1:3 scale semi-rigid steel frame with buckling-restrained steel plate shear wall to study the seismic performance of this type of structure. The results showed that the seismic resistance was adequate for survival in large seismic excitations. During the past 50 years, there is a large volume of published studies on steel plate shear walls with different design and detailing strategies. One approach employs heavily stiffened steel plate shear walls to ensure that the wall panel achieves its full plastic strength [3]. The employment of stiffened plates made of pure aluminium, with low yield strength and high ductility features [4], provides an effective dissipative capability to the whole structure, which can be controlled as a design parameter by choosing appropriate panel dimensions and varying the stiffeners arrangement [5]. Dissipative shear panel made of a low-strength material, namely the heath treated EN-AW-1050A aluminium alloy was further investigated and the obtained results signified that the buckling phenomena were mitigated compared with other more conventional shear panel typologies, characterized by the same geometry and material [6]. Tests of one story similar steel plate shear walls with and without stiffeners were carried out by Sabouri-Ghomi and Sajjadi. It was concluded that installation of stiffeners improved the behavior of the steel plate shear walls [7]. Natalia et al. [8] proposed a ring-shaped steel plate shear wall (RS-SPSW), consisting of a steel web plate cut with a pattern of holes leaving ring-shaped portions of steel connected by diagonal links. The ring shape resists out-of-plane buckling through the mechanics of a circular ring deforming into an ellipse. Eight 1:6 scaled test specimens, with two plate thicknesses and four different circular opening ratios at the center of the panel, were tested under the effects of cyclic hysteresis loading at the thin-walled structures research laboratory of Urmia University, Urmia, Iran. The obtained ductility of specimens shows the stable functioning of a system in the nonlinear range but existence of an opening at the center of the panel causes a noticeable decrease in energy absorption [9]. The hysteretic performance of steel perforated shear panels might be detrimentally influenced by pinching effects and softening. Therefore, a suitable analytical formulation for the prediction of the strength accounting for the influence of the detrimental effects and a useful predictive tool for defining the optimal perforation geometry to be adopted as a function of the expected shear demand were provided by De Matteis and Sarracco [10]. Otherwise, nonlinear seismic analysis was applied to design the perforated steel

* Corresponding author at: Key Lab of Concrete and Prestressed Concrete Structures of Ministry of Education, Southeast University, Nanjing 210096, China.
E-mail address: davidjingyu@gmail.com (J. Lu).

https://doi.org/10.1016/j.jcsr.2018.05.002
0143-974X/

plate shear walls by predicting the design forces in the columns [11]. Astaneh-Asl [12] and Kulak et al. [13] summarized the multinational research on steel plate shear walls, including design models and procedures.

Inspired by the application of concrete shear walls with seams, traced to earlier studies by Omori et al. [14] and Mutoh et al. [15] who utilized slits to improve the earthquake resistance of concrete shear walls, a brand new type of earthquake-resisting element, steel plate shear walls with slits (SPSWS) was proposed. In recent years, there has been an increasing amount of literature on SPSWS. Hitaka and Matsui [16] studied the seismic design and inelastic behavior of SPSWS which relied on ductile flexural deformations provided by the numerous slits slotted in the panel. A total of 42 specimens were tested under monotonic and cyclic lateral loading to validate the performance of the shear wall. All specimens showed large ductility. Results supported the proposed equations for calculating the strength and stiffness of the wall panels. Ke and Chen [17] came up with a calculation equation aiming at estimating the energy dissipation capacity of SPSWS and then the equation was assured by results from FEM analysis. Width versus height ratio and width versus thickness ratio were considered as the influential factors of the energy dissipation capacity of SPSWS.

Cortés and Liu [18] performed a research on steel slit panel-frame system via an experimental program, mainly focusing on the fundamental characteristics of the steel slit panels, and the behavior of the steel slit panels within the frame. The research found that all the steel slit panels (SSPs) tested in the experimental program were capable of undergoing interstory drifts of at least 5% without causing reduction in load carrying capacity below 80% of its ultimate strength. The stiffness in the SSP is clearly affected by the flexural rigidity of the beams connected to the panels. Hebdon et al. [19] proposed some advices on designing slit walls in a frame that considers the benefits of the steel slit panel frame (SSPF) such as easing of fabrication and erection, function as replaceable fuse elements, and reduce cumulative story stiffness reduction due to the SSP-frame interaction.

The steel slit damper (SSD), fabricated from a standard structural wide-flange section with a number of slits cut from the web, is an extension application of the SPSWS. Chan and Albermani [20] proposed steel slit dampers with weld-free design and analyzed its hysteretic behavior based on nine sets of tests. The results showed that the weld-free SSD yielded at a small lateral angle, which meant the large quantity of energy was absorbed in the early period of the earthquake. Jacobsen et al. [21] came up with a new passive damping device composed of steel plate with slits. Analysis demonstrated that it exhibited stable hysteretic performance with good ductility. Tests on slits dampers with frame were then carried out and results showed that this kind of system behaved excellent hysteretic performance and was recoverable after the earthquake.

Slits setting in the SPSW decreased the lateral stiffness and ultimate lateral loading capacity to some degree [22], which aroused concerns on satisfying the designing requirements for practical use. Approaches including employing diagonally stiffener [23] and adding concrete plate were adopted to ensure that the steel plate achieves the objective of excellent lateral stiffness, ultimate bearing capacity, and ductility.

In this study, two types of SPSWUSs (the papilionaceous and the fusiform) are introduced and investigated systematically for the first time. This paper aims at putting up a simple approach to improve the stiffness and loading capacity with given designing parameters. Four 1/3-scaled test specimens are designed for the experimental study. Two of them are SPSWUSs, and the others are traditional SPSWSs. The main parameters studied in this paper were energy dissipation capacity, ultimate lateral loading capacity, lateral stiffness, ductility and failure modes. Results showed that SPSWUS had better energy dissipation capacity and ductility as well as relatively higher lateral stiffness and ultimate lateral loading capacity than conventional SPSWS. Results from experimental tests and finite element analysis were compared and good correlations were observed.

2. Concept of steel plate shear wall with unequal length slits

Two types of SPSWUSs, fusiform specimen (Fig. 1(a)) and papilionaceous specimen (Fig. 1(b)) are analyzed in this study. The two specimens have the same geometrical configurations including geometric dimension, slits spacing and stiffener dimensions. For papilionaceous specimen, the length of slits increases from the middle to edge. While for fusiform specimen, the length of slits decreases from the middle to

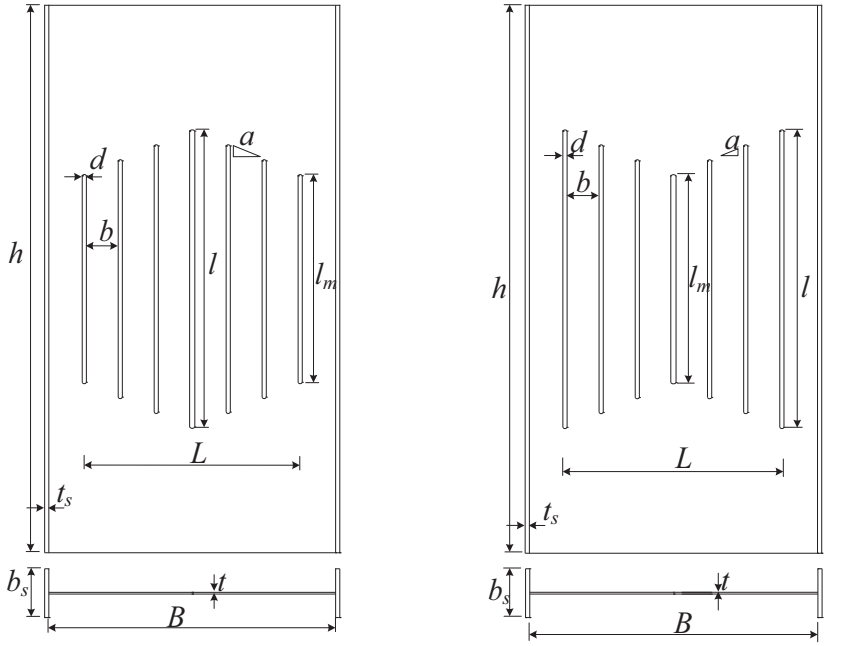

(a) Type A (fusiform specimen) (b) Type B (papilionaceous specimen)

Fig. 1. Geometrical model of steel plate shear wall with unequal length slits.

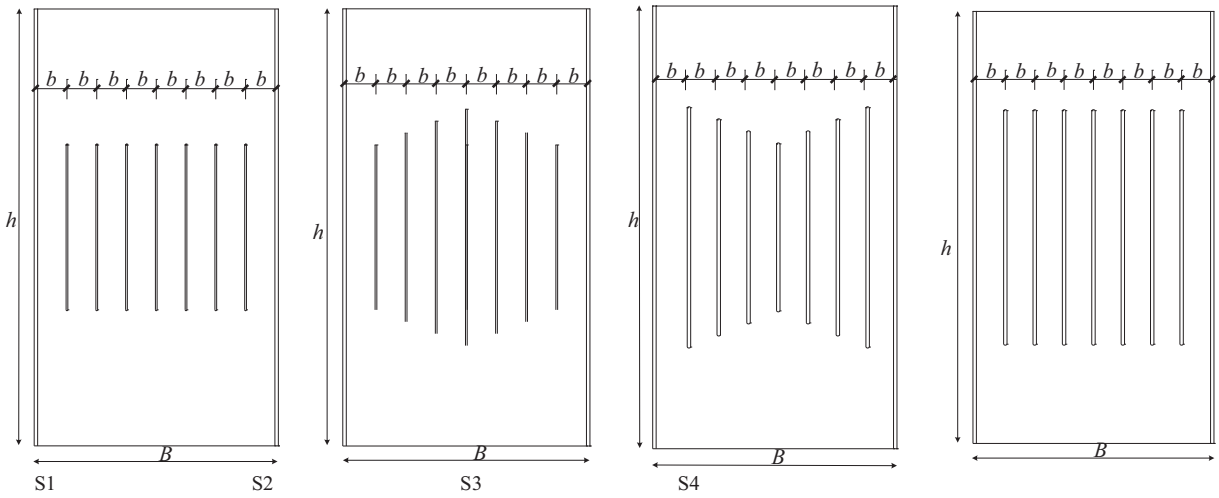

Fig. 2. Test specimens.

edge. The shortest length of slits is lm and the longest is l. While α is defined as the slope of the top edge of a series of slits.

3. Test preparation

3.1. Test specimens

Four 1/3-scaled specimens are presented in Fig. 2 and the detailed geometric parameters of the four test specimens are shown in Table 1. S1 and S4 are traditional SPSWS specimens while S2 and S3 are papilionaceous and fusiform SPSWUS specimens. The dimension of the infill steel plate ($h \times B \times t$) is 1010 mm × 550 mm × 8 mm, which satisfies the recommendation proposed by Cortes and Liu [18]. Vertical slits were created by wire cutting. Circular arcs were cut at both ends of each slit to minimize the stress concentrations. The width of the slit is 4 mm and the width of flexural links between slits is 69 mm. Considering the fact that slopes α have effect on the energy dissipation capacity of specimens, α for S2 and S3 are finally determined as −0.4 and 0.4 in radius respectively by means of FEM analysis. The left and right sides of specimens were equipped with vertical stiffeners whose dimensions are 1010 mm × 100 mm × 8 mm.

Table 1
Detailed parameters of the test specimens.

NO.	Dimension of Infill steel plate (mm)	Dimension of stiffener (mm)	l (mm)	l_m (mm)	α
S1	1010 × 550 × 8	1010 × 100 × 8	385	385	0
S2			550	385	−0.4
S3			550	385	0.4
S4			550	550	0

3.2. Test setup

As shown in Fig. 3, specimens were fixed in the test equipment by high-strength bolts. The test equipment consisted of L-shaped loading beam, ground beam, four-bar linkage and structural steel frame.

Fig. 4 presents the test setup applied in the laboratory. The horizontal load was applied on L-shaped loading beam by actuator whose upper capacity is 1000kN with an accuracy of 0.01kN. The point of loading was placed at the same level as the center of the specimen in order to counteract the overturning moment. In addition, two sets of lateral supporting frameworks were set to keep the loading beam stay in-plane.

Four linear variable differential transformers (LVDT) were arranged in the loading process: LVDT ① was used to measure the horizontal

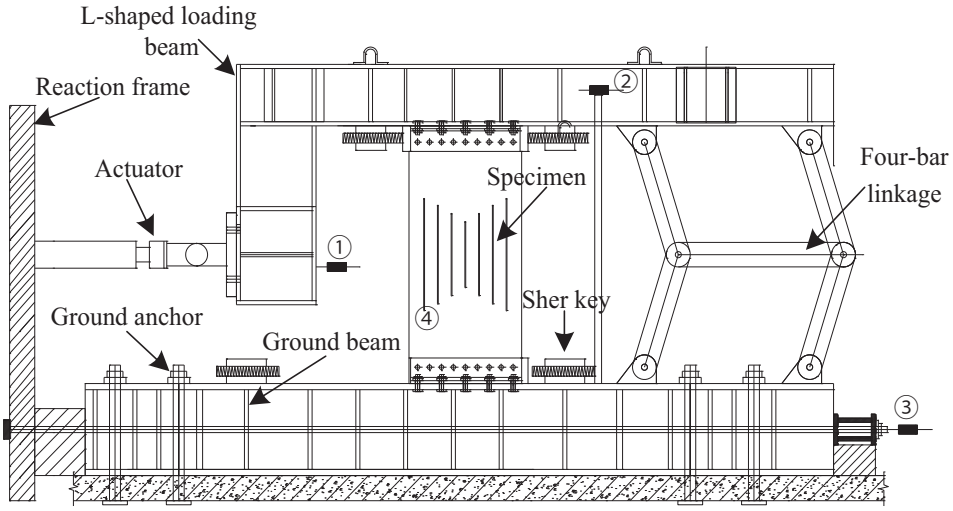

Fig. 3. Test setup and instrumentation.

(a) Front view (b) Right view

Fig. 4. Loading device in laboratory.

deformation of L-shaped loading beam. LVDT② was set to measure the horizontal displacement of loading beam which was relatively close to the real displacement of SPSWS specimens. LVDT③ mainly measured the horizontal slide of the ground beam and LVDT④ measured the out-of-plane displacement of marginal flexural links. Considering that SPSWS specimens yielded at quiet small displacement, displacement control method was chosen when applying cyclic loading. The specific loading system is shown in Fig. 5. The target displacement in each loading level was determined as multiple of the yield displacement and two complete cycles were applied for each loading level.

4. FEM analysis

4.1. Finite element models

FEM analysis was applied to predict the mechanical behavior of the specimens and determine the yield displacement in each loading level. ABAQUS® software was chosen in this study to analyze the four specimens. Both the infill steel plate and stiffener were meshed with four-node, reduced integration shell elements S4R [24]. The grid at end of the slits was subdivisionally meshed to improve the precision (shown in Fig. 6). A bilinear constitutive model was used for steel material based on the result of material characteristic test. From the test result, yield strength (σ_y) of steel is 266 N/mm^2 and the Poisson's ratio (μ) is 0.3. Considering the Bauschinger effect of steel, a bilinear kinematic hardening model was adopted under low cycle loads. The elasticity modulus (E_s) was 2.06×10^5 N/mm^2 and the tangent modulus (E_t) was defined as $0.01E_s$ (as shown in Fig. 7).

4.2. Boundary constraint and initial imperfection

The bottom edge of the specimen was completely constrained while for the top edge of specimen, the horizontal and vertical translations DOFs were released. In order to avoid stress concentration throughout the loading process, a rigid beam was set at the top of the specimen. The grid beam and SPSWS specimen were tied when simulated in ABAQUS®. The first buckling mode was selected to simulate the initial

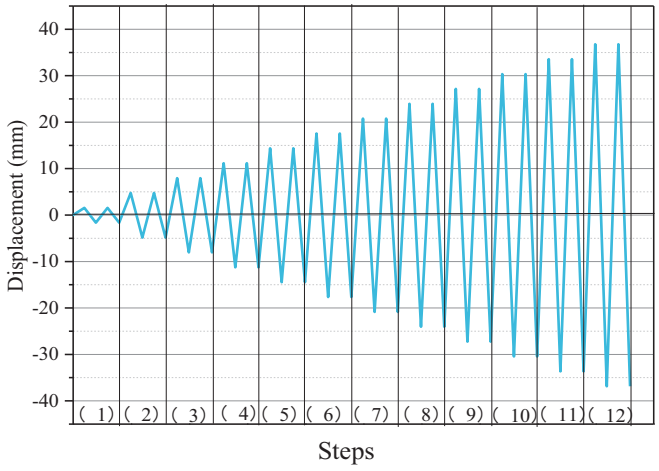

Fig. 5. Loading system.

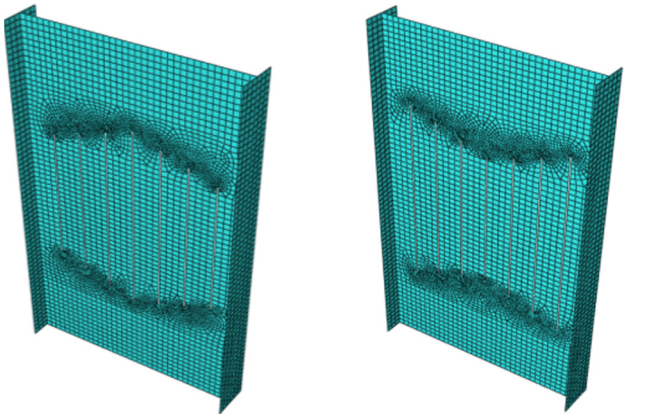

(a) Fusiform specimen (S2) (b) Papilionaceous specimen (S3)

Fig. 6. FEM models.

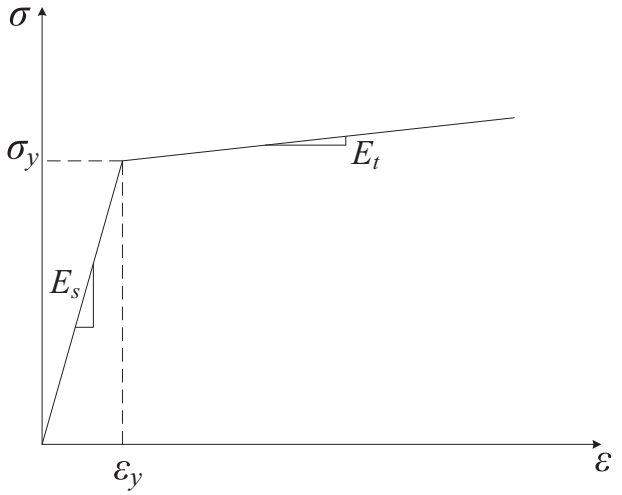

Fig. 7. Constitutive relationship.

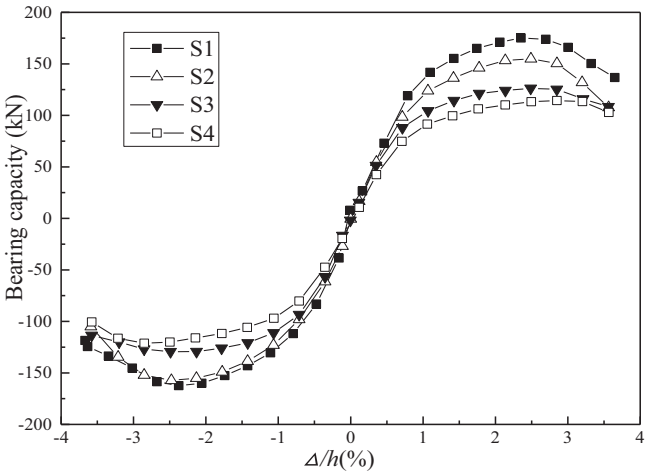

Fig. 9. Skeleton curves.

imperfections of the specimens and the amplitude of the defect was determined by the tests [25].

5. Test results

5.1. Hysteretic behavior

Fig. 8 shows the hysteretic curves of four specimens obtained from FEM analysis. All the hysteretic curves of specimens are plump while the lateral drift angle (Δ/h) is less than 2% (2% is the elastic plastic inter-story drift index in Current China Seismic Design Code of Buildings [26]), after which a pinch phenomenon appears with the load increasing. Pinch phenomenon of S1 is most obvious and its hysteretic curve turns fusiform into S-shape as load increases. On the contrary, pinch phenomenon of S4 is not so obvious compared with others.

The ultimate bearing capacity of S1 is higher but the corresponding Δ/h is small. S1 shows poor ductility as its hysteretic curve drops obviously when the Δ/h is close to 2%. In contrast, hysteretic curve of S4 drops slowly which shows good ductility. It shall be noted that S4 has the lowest ultimate loading capacity, which means smaller area within the hysteretic loop. S4 can absorb less energy in an earthquake when compared with other SPSWUS specimens. By contrast, S2 and S3 have better ductility than S1 and owns higher ultimate bearing capacity and energy dissipation capacity than S4.

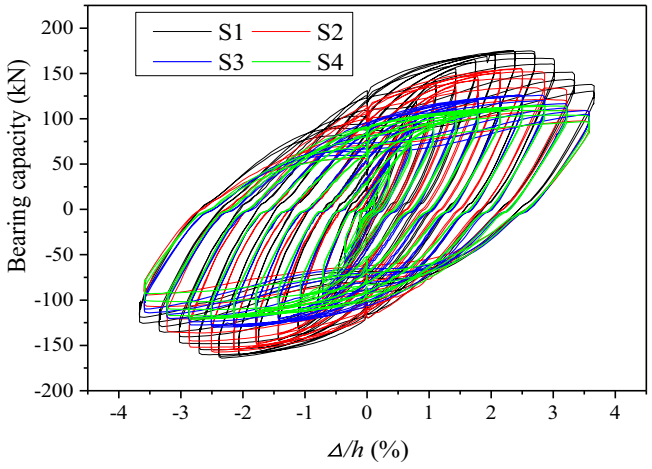

Fig. 8. Hysteretic curves of four specimens.

5.2. Skeleton curves and mechanical parameters

Skeleton curves are formed by the peaks of hysteretic curves in each cycle. Fig. 9 represents the skeleton curves of the four specimens and Table 2 lists their characteristic parameters. It is obvious that initial stiffness of the four specimens is in the order of S4 < S2 < S3 < S1 and the ultimate load bearing capacity of the four specimens can be sequenced as S4 < S3 < S2 < S1. The initial stiffness of S1 is almost 17 times higher than S4's and the ultimate load bearing capacity of it is 1.53 times higher than S4's. Comparing the long slits specimen S4, SPSWUSs possess on average 1.36 times higher initial stiffness and 1.23 times better ultimate bearing capacity. Otherwise, load bearing capacity of all specimens shows a decline at the later loading stage. Especially, the load bearing capacity of S1 and S2 decreases sharply after reaching the peak while the curves of S3 and S4 fall slowly. It is indicated that S3 and S4 own better ductility.

5.3. Energy dissipation capacity

Energy dissipation capacity refers to the structure or component's ability of absorbing energy after plastic deformation in earthquake action. Energy dissipation capacity can be assessed by Energy dissipation coefficient (E) which can be calculated by Eq. (1) [27].

$$E = \frac{S_{ABC} + S_{CDA}}{S_{OBF} + S_{ODE}} \tag{1}$$

In the equation, S_{ABC}、S_{CDA} are the areas enclosed by hysteretic curves and x axis, respectively while S_{OBF}、S_{ODE} are the areas of OBF and ODE, respectively (Fig. 10).

Table 2
Characteristic parameters.

NO.	Direction	Initial stiffness	Ultimate bearing capacity	Coefficient of ductility
		kN/mm	P_u/kN	μ
S1	Positive	29.38	175.09	2.45
	Negative		−162.45	2.60
S2	Positive	21.95	154.84	2.35
	Negative		−157.27	2.43
S3	Positive	25.01	126.21	2.95
	Negative		−129.40	3.12
S4	Positive	17.22	114.34	3.25
	Negative		−121.17	2.63

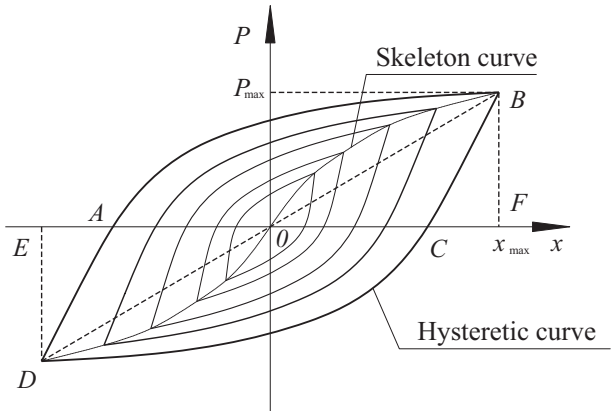

Fig. 10. Typical hysteretic curves.

Fig. 11 presents the relationship between the E and Δ/h of four specimens. It can be clearly seen that the energy dissipation coefficient E of S1 and S2 are relatively lower than the other two specimens. E of S1 shows a sudden decline when the lateral angle is close to 2.5%. As load increases, The E values of all specimens increases slowly and eventually decline because of the out-of-plane buckling of the flexural links. S3 has the highest E value when the Δ/h is less than 2%, which indicates that the energy dissipation capacity of S3 is better than other specimens.

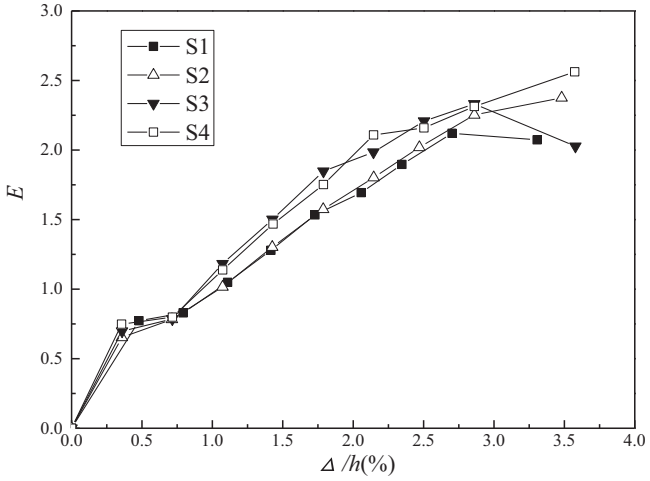

Fig. 11. Variation of energy dissipation coefficient.

5.4. Test phenomenon

The failure modes of all four specimens were discussed as follows. During the testing of S1, a noise was heard when the Δ/h reached 0.5% and the bearing capacity was controlled by its shear bearing capacity. Flexural links exhibited an obvious 'S' shape in this loading process. The deformation of specimen was mainly in the form of in-plane bending up to a lateral angle of 1.13%. When the Δ/h reached 2.38% (Fig. 12(a)), flexural links produced an obvious out-of-plane buckling and its bearing capacity decreased correspondingly. Cracks appeared near the upper end of the left slits when the Δ/h reached 2.86% (Fig. 12(b)). Cracks spread as load increased, which led to an obvious pinch phenomenon appeared in hysteretic curves. In the last loading cycle, flexural links produced an obvious out-of-plane deformation and the cracks were much more developed (Fig. 12(c)).

A noise was heard when the Δ/h reached approximately 0.71% for S2 specimen. Small deformation also appeared at that time. Flexural links produced an obvious in-plane bending deformation when the Δ/h reached 1.07%. The plasticity developed adequately at the end of flexural links. Then edge flexural links produced an obvious out-of-plane buckling when the Δ/h reached 2.50% (Fig. 13(a)). The maximum out-of-plane deformation of edge flexural links is 5.0 mm at that time, a decline was observed in its skeleton curve at this moment. As load increased, the central flexural links started to produce obvious out-of-plane buckling. The upper and lower end of right slits produced cracks when the Δ/h reached 2.85% (Fig. 13(b)). Correspondingly, its hysteretic curves showed obvious pinch phenomenon. In the last loading cycle, flexural links produced obvious out-of-plane deformation and cracks spread evidently as shown in Fig. 13-(c). At the end of loading process, bearing capacity of S2 decreased to 61% of its ultimate load bearing capacity.

Plasticity of flexural links in S3 developed adequately when the Δ/h was less than 1.07%, its phenomenon was similar to that of S2. Edge flexural links produced small out-of-plane deformation when the Δ/h reached 1.43%. Maximum out-of-plane deformation of edge flexural links was only 2.0 mm which indicated that the deformation was mainly in the form of in-plane bending. Out-of-plane deformation increased slowly with the increasing of the load. All flexural links produced obvious out-of-plane buckling almost at the same time. The load bearing capacity started to decrease in skeleton curve correspondingly when the Δ/h reached 2.50% as shown in Fig. 14(a). Edge flexural links started to produce micro cracks when the Δ/h reached 3.2%. With load increasing, cracks spread gradually as shown in Fig. 14(b), and hysteretic curves showed a pinch phenomenon. However, the pinch phenomenon was not as obvious as S1 and S2. In the last loading cycle, flexural links produced an obvious out-of-plane deformation and cracks spread obviously (Fig. 14(c)). The bearing capacity of S3 decreased to 77.7% of its

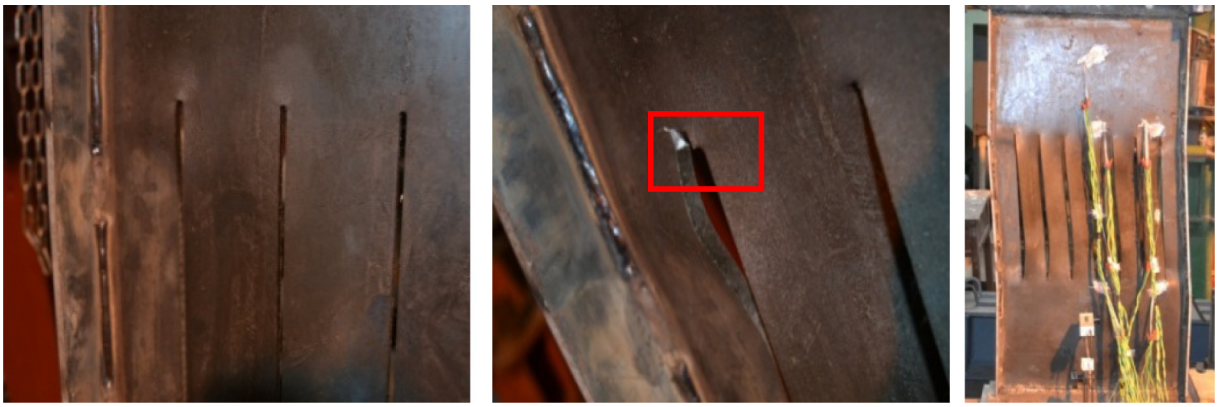

(a) Initial deformation (b) Cracks appeared (c) Failure mode

Fig. 12. Test phenomenon of S1.

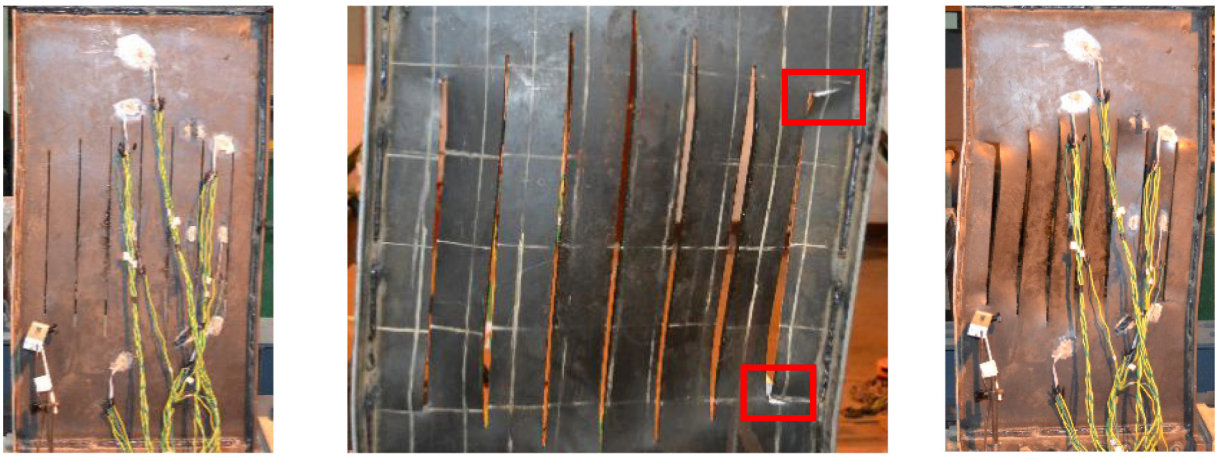

(a) Initial deformation (b) Cracks appeared (c) Failure mode

Fig. 13. Test phenomenon of S2.

ultimate bearing capacity which indicated that S3 still had high load bearing capacity and good energy dissipation capacity in the last loading cycle.

When the Δ/h reached 1.43%, the stiffener of S4 started to present obvious S-shape. The relative displacement between the upper and the lower of specimen was quite noticeable. Maximum out-of-plane deformation of left flexural links was 1.0 mm which indicated that the deformation was mainly bending in plane. With the load increasing, out-of-plane deformation of edge flexural links increased slowly. The infill steel plate started to produce obvious out-of-plane deformation when

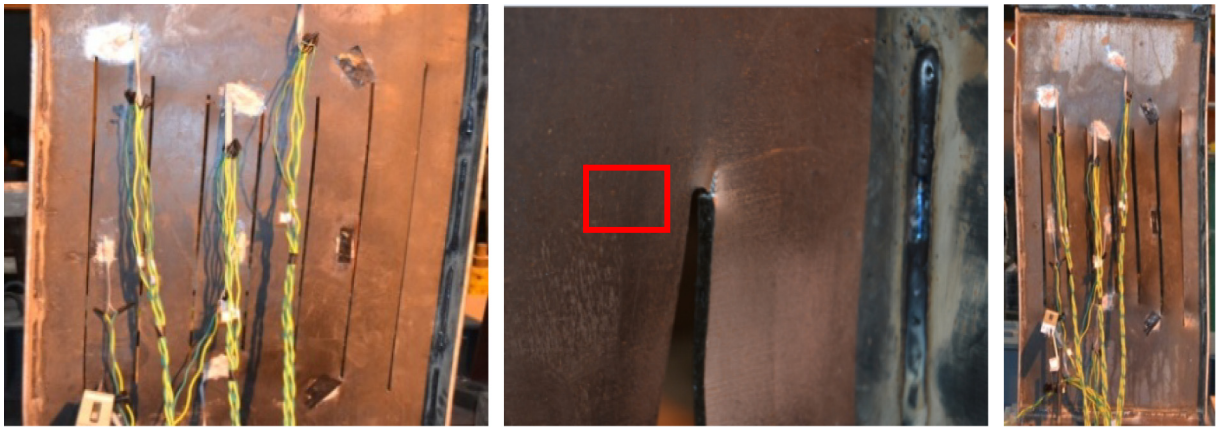

(a) Initial deformation (b) Cracks appeared (c) Failure mode

Fig. 14. Test phenomenon of S3.

(a) Initial deformation (b) Cracks appeared (c) Failure mode

Fig. 15. Test phenomenon of S4.

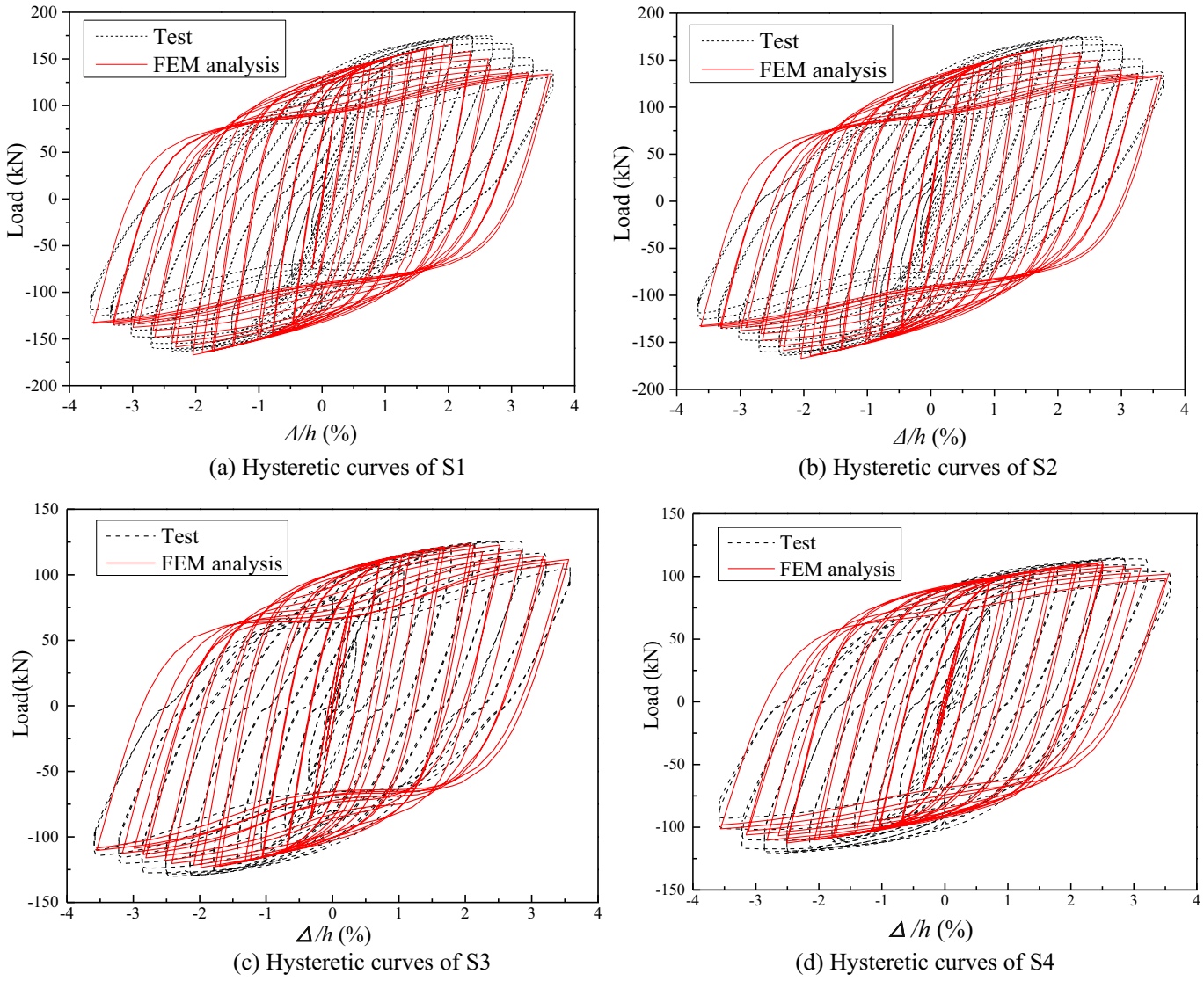

Fig. 16. Hysteretic curves of tests and FEM analysis.

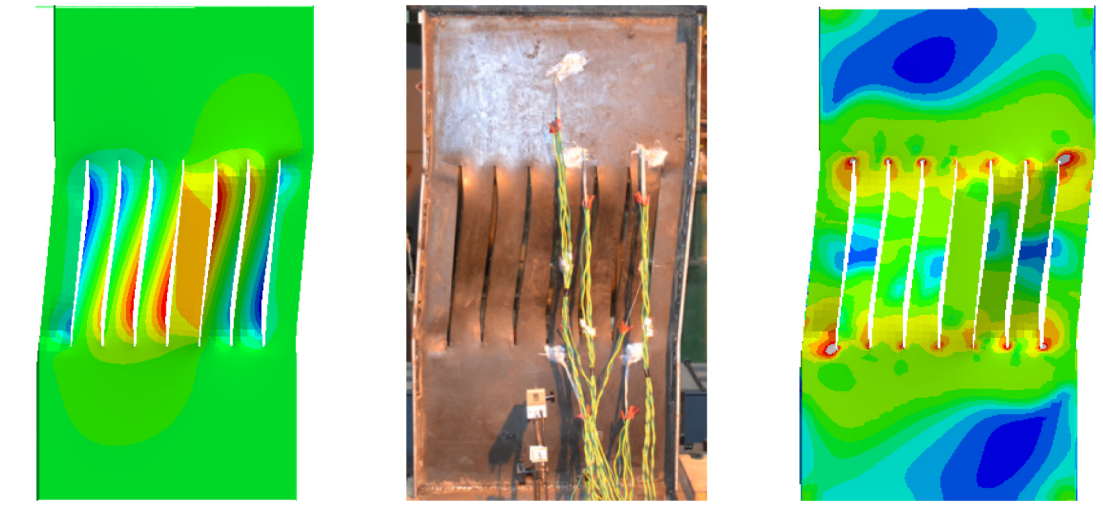

Fig. 17. Failure mode comparison of S1 ($\Delta = 3.64\%$).

(a) Deformation in FEM analysis (b) Deformation in test (c) Mises stress distribution

Fig. 18. Failure mode comparison of S2 ($\Delta = 3.56\%$).

the Δ/h reached 3.2% as shown in Fig. 15(a). Edge flexural links started to produce out-of-plane buckling and its maximum deformation was up to 4.0 mm, which led to the E declined quickly as the Δ/h approached 3%.Cracks appeared at the upper end of the edge marginal flexural links as load increased (Fig. 15(b)). In the last loading cycle, flexural links produced obvious out-of-plane deformation and its hysteretic curve showed serious pinch phenomenon as shown in Fig. 15(c).

5.5. Comparisons of hysteretic curves

Comparisons of hysteretic curves from experiment and FEM analysis are showed in Fig. 16. As the loading condition in FEM analysis is more ideal, hysteretic curves of FEM analysis is plumper than those from tests. The load bearing capacity is higher than that of tests as well. Generally, variation trend of experimental results is similar to that of the FEM analysis, which indicates that the element selection and the boundary condition assumption are reasonable for this kind of study.

5.6. Comparisons of deformation and failure mode

Out-of-plane deformation of testing specimens and FE models are showed in Figs. 17–20 with Von Mises stress contour plot from FEM. Failure modes of testing specimens are mainly in the form of out of plane flexural-torsional buckling, which is similar to that of FEM analysis. The maximum Von Mises stresses of S1, S2 and S4 mainly occurs at the end of edge slits. Then cracks appear nearby and spread quickly, which decreases their bearing capacity and energy dissipation capacity. In this case, Von Mises stress in the middle of flexural links was lower than the edge links, and its energy dissipation capacity cannot be fully utilized. Lateral stiffness of the central flexural links in S3 was higher, which decreases stress concentration of edge flexural links and thus

(a) Deformation in FEM analysis (b) Deformation in test (c) Mises stress distribution

Fig. 19. Failure mode comparison of S3 ($\Delta = 3.64\%$).

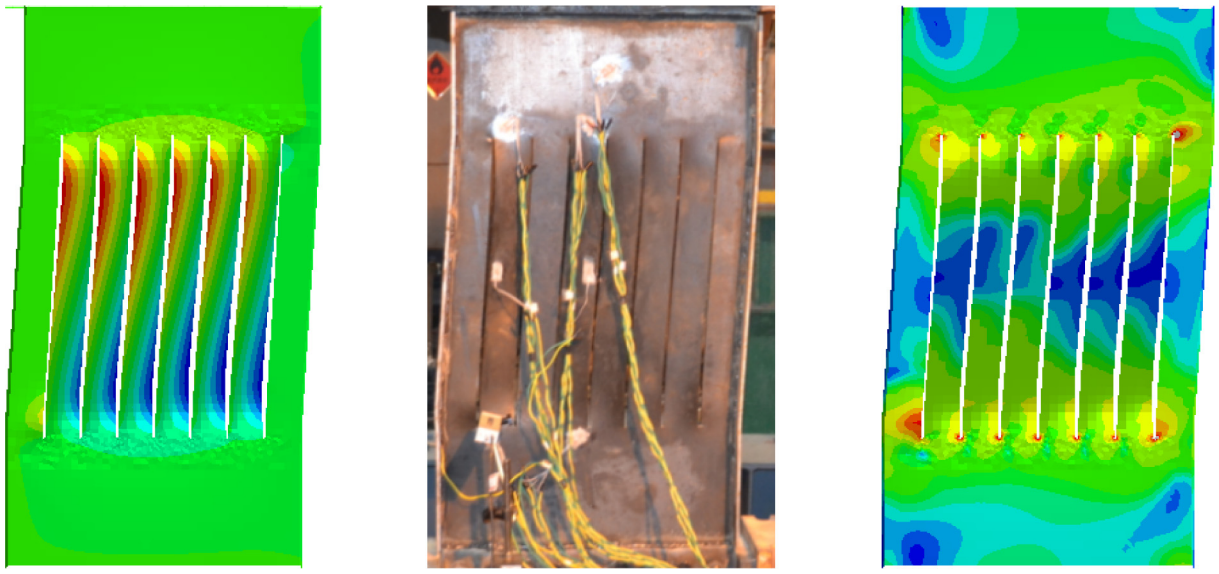

(a) Deformation in FEM analysis (b) Deformation in test (c) Mises stress distribution

Fig. 20. Failure mode comparison of S4 ($\Delta = 3.64\%$).

its energy dissipation capacity can be fully utilized. It is clear that stress distribution near the end of flexural links in S3 is uniform, which corresponds to higher energy dissipation capacity.

6. Conclusion

Two types of SPSWUSs, fusiform specimen (S2) and papilionaceous specimen (S3) were analyzed by means of FEM analysis and low cyclic loading tests in this paper. The effect of different types of shear walls on lateral stiffness, ultimate bearing capacity, energy dissipation capacity and hysteretic behavior was discussed in detail. Tests were carried out to validate the rationality of FEM analysis in terms of boundary condition and element selection. A comparison between numerical analysis and laboratory tests shows excellent agreement. Conclusions can be drawn as follows:

(1) Among the two traditional SPSWS specimens (S1 and S4), fusiform specimen (S2) and papilionaceous specimen (S3), the lateral stiffness and ultimate load bearing capacity of S4 were the lowest. The lateral stiffness was about o.7 times lower and the ultimate load bearing capacity was o.8 times lower than S2 and S3 on average. It meant changing the shapes of slits cutting in the shear walls could be an effective way to improve the lateral stiffness and ultimate load bearing capacity.

(2) Additionally, the energy dissipation coefficient of S2 was nearly close to that of S1 and was relatively the lowest, while the energy dissipation coefficient of S3 was the highest when under the circumstance of satisfying the elastic plastic inter-story drift index 2% stipulated in Current China Seismic Design Code of Buildings. In the meanwhile, S3 owned excellent ductility, 1.27 times better than S2, and relatively high lateral stiffness, ultimate load bearing capacity. It was indicated that the papilionaceous SPSWUS could be a good choice for designers choosing slit walls.

(3) It was found that all the flexural links of S3 emerged out-of-plane buckling almost simultaneously, while for the other three walls, out-of-plane deformation at the edge flexural links were prior to the deformation of the central flexural links. It was indicated that the energy dissipation capacity of flexural links was better utilized in S3 and thus the mechanical properties as well as hysteretic performance of S3 were improved from the others.

(4) The hysteretic curves of FEM analysis were plumper than those of tests because the loading condition was idealized and cracks were not taken into consideration in FEM analysis, Results from FEM analysis and tests coincided reasonably well with each other, despite the fact that installation imperfection or slippage of testing frame were associationally occurred.

Acknowledgements

The research was supported by the National Natural Science Foundation of China (Grant no. 51778129), Prospective Joint Research Project of Jiangsu Province, China (Grant no. BY2016076-06), the Natural Science Fund Project in Jiangsu Province, China (Grant no. BK20161422). This financial support is gratefully acknowledged.

References

[1] M. Wang, W.G. Yang, Hysteretic behaviors study of thin steel plate shear wall structures, J. Build. Struct. 36 (1) (2015) 68–77.
[2] M.L. Ge, J.P. Hao, J.G. Yu, P.Z. Yan, S.C. Xu, Shaking table test of buckling-restrained steel plate shear walls, J. Constr. Steel Res. 137 (2017) 254–261.
[3] Y. Takahashi, Y. Takemoto, T. Takeda, M. Takeda, Experimental study on thin steel shear walls and particular bracing under alternative horizontal load, Preliminary Rep, IABSE Symposium on Resistance and Ultimate Deformability of Structures Acted on by Well-defined Repeated Loads, International Association for Bridges and Structural Engineering, Lisbon, Portugal, 1973.
[4] G. De Matteis, F.M. Mazzolani, S. Panico, Experimental tests on pure aluminium shear panels with welded stiffeners, Eng. Struct. 30 (6) (2008) 1734–1744.
[5] G. De Matteis, G. Brando, S. Panico, F.M. Mazzolani, Bracing type pure aluminium stiffened shear panels: an experimental study, Int. J. Adv. Steel Constr. 5 (2) (2009) 106–119.
[6] G. Brando, F. D'Agostino, G. De Matteis, Experimental tests of a new hysteretic damper made of buckling inhibited shear panels, Mater. Struct. 46 (12) (2013) 2121–2133.
[7] S. Sabouri-Ghomi, S.R.A. Sajjadi, Experimental and theoretical studies of steel shear walls with and without stiffeners, J. Constr. Steel Res. 75 (2012) 152–159.
[8] E. Natalia, Matthew R. Eatherton, M. Abhilasha, Experimental study of ring-shaped steel plate shear walls, J. Constr. Steel Res. 103 (2014) 179–189.
[9] H. Valizadeh, M. Sheidaii, H. Showkati, Experimental investigation on cyclic behavior of perforated steel plate shear walls, J. Constr. Steel Res. 70 (2012) 308–316.
[10] G. De Matteis, G. Sarracco, G. Brando, Experimental tests and optimization rules for steel perforated shear panels, J. Constr. Steel Res. 123 (2016) 41–52.
[11] A.K. Bhowmick, G.Y. Grondin, R.G. Driver, Nonlinear seismic analysis of perforated steel plate shear walls, J. Constr. Steel Res. 94 (2014) 103–113.
[12] A. Astaneh-Asl, Seismic Behavior and Design of Steel Shear Walls, Steel Tips, Structural Steel Education Council, Moraga, California, 2001.
[13] G.L. Kulak, Steel plate shear walls—an overview, Engl. J. 38 (1) (2001) 50–62.

[14] S. Omori, K. Toyam, T. Cho, T. Takahashi, Test on RC shear wall with slits, Summaries of Technical Papers of Annual Meeting AIJ, 1966 (Kanto, Japan).
[15] K. Mutoh, O. Miyashita, M. Osada, H. Kanayama, Stress and deformation of slit wall, using FEM, Summaries of Technical Papers of Annual Meeting AIJ, 1968 (Chugoku, Japan).
[16] T. Hitaka, C. Matsui, Experimental study on steel shear wall with slits, J. Struct. Eng. ASCE 129 (5) (2003) 586–595.
[17] K. Ke, Y.Y. Chen, Design method of steel plate shear wall with slits considering energy dissipation, The 15th World Conference of Earthquake Engineering, 2012 (Shanghai, China).
[18] G. Cortés, J. Liu, Experimental evaluation of steel slit panel–frames for seismic resistance, J. Constr. Steel Res. 67 (2011) 181–191.
[19] M. Hebdon, J. Lloyd, J. Liu, Practical design considerations for steel slit panel frames, Structures Congress ASCE 2012, pp. 1577–1585.
[20] R. Chan, F. Albermani, Experimental study of steel slit damper for passive energy dissipation, Eng. Struct. 30 (2008) 1058–1066.
[21] A. Jacobsen, T. Hitaka, M. Nakashima, Online test of building frame with slit-wall dampers capable of condition assessment, J. Constr. Steel Res. 66 (11) (2010) 1320–1329.
[22] L. Jiang, Y.Y. Chen, W.D. Wang, Research on elastic lateral stiffness and simplified model of steel plate shear wall with slits, J. Arch. Civ. Eng. 27 (3) (2010) 115–120.
[23] E. Alavi, F. Nateghi, Experimental study of diagonally stiffened steel plate shear walls, J. Struct. Eng. 139 (11) (2013) 1795–1811.
[24] P.M. Clayton, C.Y. Tsai, J.W. Berman, Comparison of web plate numerical models for self-centering steel pate shear walls, Earthq. Eng. Struct. Dyn. 44 (12) (2015) 2093–2110.
[25] Y.B. Zhong, S.M. Zhang, X.B. Ma, Research of shear resistance static behaviors of steel-plate shear walls with slits, J. Harbin Inst. Technol. 38 (12) (2006) 2054–2059.
[26] Of the People's Republic of China national standard building seismic design code GB50011–2010.
[27] L.H. Guo, X.B. Ma, S.M. Zhang, Experimental research on steel plate shear wall with slits, Eng. Mech. 29 (3) (2012) 133–142.